Modulated Crystalline-B Phases in Liquid Crystals

Modulated crystalline-*B* phases in liquid crystals

E. B. Sirota,* P. S. Pershan, and M. Deutsch†
Department of Physics, Harvard University, Cambridge, Massachusetts 02138
(Received 12 January 1987)

Detailed x-ray scattering studies of the modulated phases of 4-*n*-heptyloxybenzylidene-4-*n*-heptylaniline (7O.7) are reported. In addition to the previously identified one-dimensional modulation that appears at the transition from the crystalline-*B* (Cr*B*) phase with *ABAB* stacking to the Cr*B* phase with orthorhombic stacking, there are two other modulation structures each of which contains two noncolinear modulations. The modulations are explained in terms of a phenomenological model in which domains are separated by walls for which the intralayer packing is identical to the lower-temperature crystalline-*G* phase. This model yields the measured values for both the modulation wave vector and the lattice distortion.

INTRODUCTION

The present study involves the material 4-*n*-heptyloxybenzylidene-4-*n*-heptylaniline usually referred to as 7O.7. A companion paper[1] describes the 7O.7 phase diagram and its thickness dependence. The restacking transitions in the crystalline-*B* (Cr*B*) phases of 7O.7 and similar compounds have been studied by different groups.[2–8] The stacking sequence in the Cr*B* phases of 7O.7 was found to be the following sequence:[9,10] 55°→hexagonal-*AAA* (*AAA*)→61° →monoclinic-*C* (mono)→61.5°→orthorhombic-face-centered (ortho or Or)→64°→hexagonal-close-packed-*ABAB* (*ABAB*) →69°C. The Cr*B* phases below the *ABAB* phase were reported to have a single one-dimensional modulation structure, polarized normal to the smectic layers, with a wave vector in the plane of the layers.[6,7,4,5,11,9] The modulation structure observed in the Cr*B* phases of the homologous compound 4-(*n*-pentyl)oxybenzylidene-4′-(*n*-hexyl)aniline (5O.6) was similar[12,13] and those results led to the development of a dislocation model for the modulations by Hirth *et al.*[14] That model, however, did not explain the magnitude of the modulation wave vector and did not relate to any specific model of the local interactions.

In very sensitive calorimetry measurements, Thoen and Seynhaeve[15] were able to detect the restacking transitions. In addition to the transitions observed by Collet *et al.*,[9,10] they found evidence for an additional transition between 61.5 and 64 °C. This prompted the present study in which two additional modulation structures denoted as *m*2 and *m*3 were identified. The structure reported by Collett is designated as *m*1. We will describe these structures below. The sequence of Cr*B* phases of 7O.7 is then shown to be the following: 55°→*AAA*-*m*2 or -*m*3→61°→mono-*m*2 or -*m*3→61.5°→ortho-*m*2 →62.5°→ortho-*m*1→64°→*ABAB*→69 °C. (Depending on sample history, the *AAA* and mono phases exhibit either the *m*2 or *m*3 structure.) We will propose a phenomenological model that explains the modulation structures as well as the magnitude of the wave vector. We also show how this is related to the model previously proposed by Hirth *et al.*[14]

In addition to the phase diagram for bulk 7O.7 (thick films), the thickness dependence has been measured and is reported in the companion paper.[1] The phase diagram in Fig. 1 shows the results of all those measurements.[16]

The intensity of satellites that are induced on a Bragg peak with reciprocal-lattice vector **Q**, by a modulation with wave vector **q**, amplitude $|\mathbf{u}|$, and polarization $\hat{\mathbf{u}}$ is proportional to $(\mathbf{Q}\cdot\mathbf{u})^2$ (for small values of the amplitude). The satellites are located in reciprocal space at $\mathbf{Q}\pm\mathbf{q}$. We note here that the condition for the satellites to have resolution-limited Bragg peaks is that the modulation be coherent over a range that is long in compar-

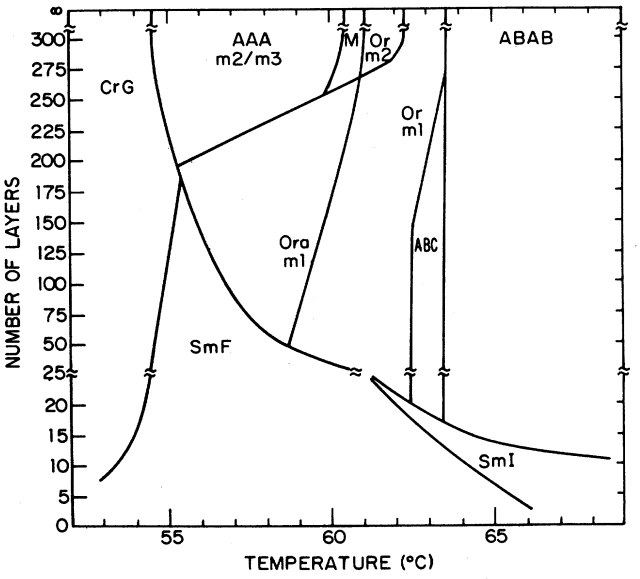

FIG. 1. Thickness-dependent phase diagram of 7O.7 [revised from Sirota *et al.* (Ref. 16)]. Phases occurring in thin films but not bulk in the temperature range shown are smectic-*I* (Sm*I*), smectic-*F* (Sm*F*), and hexagonal-*ABC* (*ABC*). Thin-film phases at higher temperatures have been studied as well (Ref. 30).

ison with the reciprocal of the width of the resolution function. Local variations in either the amplitude or the phase of the modulation, with only short-range correlations in those variations, will affect the intensity of the satellites and will not broaden them.

EXPERIMENTAL TECHNIQUES

This work involved three separate measurements at the Harvard Materials Research Laboratory rotating-anode x-ray facility on the 12-kW Rigaku RU-200 rotating-anode x-ray generator, using Cu $K\alpha_1$ radiation ($\lambda = 1.540$ Å) with an effective source size of 0.3×0.3 mm.[2] The generator was operated at 4.5 kW (50 kV, 90 mA). The sample and scattering-angle rotations were done using a Huber two-circle goniometer. Temperature control of both ovens was accomplished using a computer-settable temperature controller.[17,18] The experiments were controlled using a PDP 11/34 computer with CAMAC interface hardware for counting and motor control.

Our sample of 4-*n*-heptyloxybenzylidene-4-*n*-heptylaniline (7O.7) was obtained from CPAC Organix, Inc. In order to guarantee that we were not observing impurity-induced phenomena, part of the batch was recrystalized using petroleum ether as a solvent. While the transition temperatures seemed to vary between batches (< 1 °C), the phase sequences described here were not effected.

The reciprocal-space axes are defined relative to the layers. H and K are in the plane of the layers and have units of $4\pi/\sqrt{3}a = 1.4357$ Å^{-1}, where the nominal in-plane nearest-neighbor distance $a = 5.05$ Å. L is normal to the plane of the layers and has units of $2\pi/c = 0.2053$ Å^{-1} where the molecular length is taken to be equal to the nominal layer spacing at the highest-temperature CrB phase (69 °C), $c = 30.6$ Å.

The first of the three measurements was undertaken to obtain a precise determination of the smectic interlayer spacing d across the various CrB transitions. The model proposed by Hirth *et al.*[14] implied that the molecules remained normal to smectic layers that were locally tilted by an angle $\phi/2 = 2.75°$ with respect to the macroscopic, or average layer normal. Consequently, according to this model, the average layer spacing $\bar{d} = d\cos\phi$. Since one implication of the model was that ϕ varied across the transitions, a high-resolution triple-axis spectrometer was used to measure $\bar{d}$. A pair of germanium {220} crystals used as monochromator and analyzer, gave a full width at half maximum (FWHM) for a 2θ scan through the (001) Bragg peak, of 0.006° in a nondispersive geometry. The (001) x-ray peak corresponded to $2\theta = 2.885°$; so the longitudinal resolution FWHM, $\Delta Q_z/Q_z = \Delta 2\theta/2\theta = 0.002$. Since the peak position can be detected to about $\frac{1}{10}$ of the FWHM, molecular tilts of the order of $1.5° = \cos^{-1}(1-0.002)$ can be determined. The sample was contained by a beryllium cell that was inserted into a two-stage oven.[17,18] The oven was fitted with a cobalt samarium permanent magnet that provided an aligning field of 4.3 kG. The transverse out-of-plane resolution, determined by slits was $\sim 1°$.

The second measurement was for the purpose of characterizing the satellite structure near the (001) peak of a bulk powder sample. The same oven mentioned above was used, but without the magnets. The monochromator was a [200]LiF crystal with a rocking curve (measured with a very-high-resolution monochromator) that had a FWHM of 0.045°. The angular distribution of the incident radiation on the sample was limited to $\sim 0.03°$ by the effective horizontal x-ray source size of 0.3 mm and the 0.3-mm horizontal slit, 60 cm from the source, in front of the sample. The illuminated portion of the sample was 0.3 mm wide, 2.3 mm high, and the sample was 2.5 mm thick. A Braun OED-50 position-sensitive proportional counter was used as a detector. It contained a carbon-coated quartz wire and had an operational length of 5 cm and height of 1 cm with spatial resolution of 25 channels/mm. Data were collected in a LeCroy 3001 multichannel analyzer and read into the computer through a CAMAC interface. The detector was located 700 mm from the sample. The contribution to the 2θ resolution determined by the spot size and the detector position can be computed to be $\sim 0.03°$. The 2θ resolution was a combination of this and the angular spread in the incident beam. The 2θ resolution determined from the angular width of the Bragg peaks was measured to be $\sim 0.05°$ FWHM. The vertical resolution was $\sim 1°$ and was limited by the 1-cm height of the detector. To assure that a powder average was being taken, the sample was slowly rotated during the course of a measurement. Although the sample was unoriented, precluding measurement of the orientation of the modulation wave vector $\mathbf{q}$ with respect to the main Bragg vector $\mathbf{Q}$, the 2θ resolution was sufficiently narrow to separate the principal (001) smectic peaks at $\mathbf{Q}$ from those at $\mathbf{Q}+\mathbf{q}$. This resolution, however, was not sufficient to study the satellites on the ($10L$)-type peaks.

The third measurement was undertaken to study details of the orientation of the modulation structure relative to the nearly hexagonal in-plane symmetry. This was accomplished using the alignment obtained with freely suspended films.[2,19] Typical mosaic spreads of the layer normal were less than 0.03° and the intralayer domain size was typically of the order 1 mm^2. Although this geometry allowed easy access to the satellites on the ($10L$) peaks, it precluded study of the (001) peaks that were studied with the bulk samples. In order to observe the (001) peak in this geometry, the x-ray beam would require angular access at grazing angles ($\sim 1.5°$) to the film. This was not possible with our present oven. The oven has been described in Collett *et al.*[10] and in the companion paper.[1] The films were drawn on microscope cover glasses across a 7-mm-diam. polished hole. There is a rotation stage inside the oven that allowed the film to rotate about its normal (χ) bringing the desired domains into the scattering plane.

The films were drawn in the smectic-A (SmA) phase and cooled at about 1 °C/h into the CrB phase. When the samples were cooled into the tilted crystalline-G (CrG) phase, the mosaic of the layer normals became extremely poor. Therefore, it was not practical to examine the orientation of the satellites in that phase.

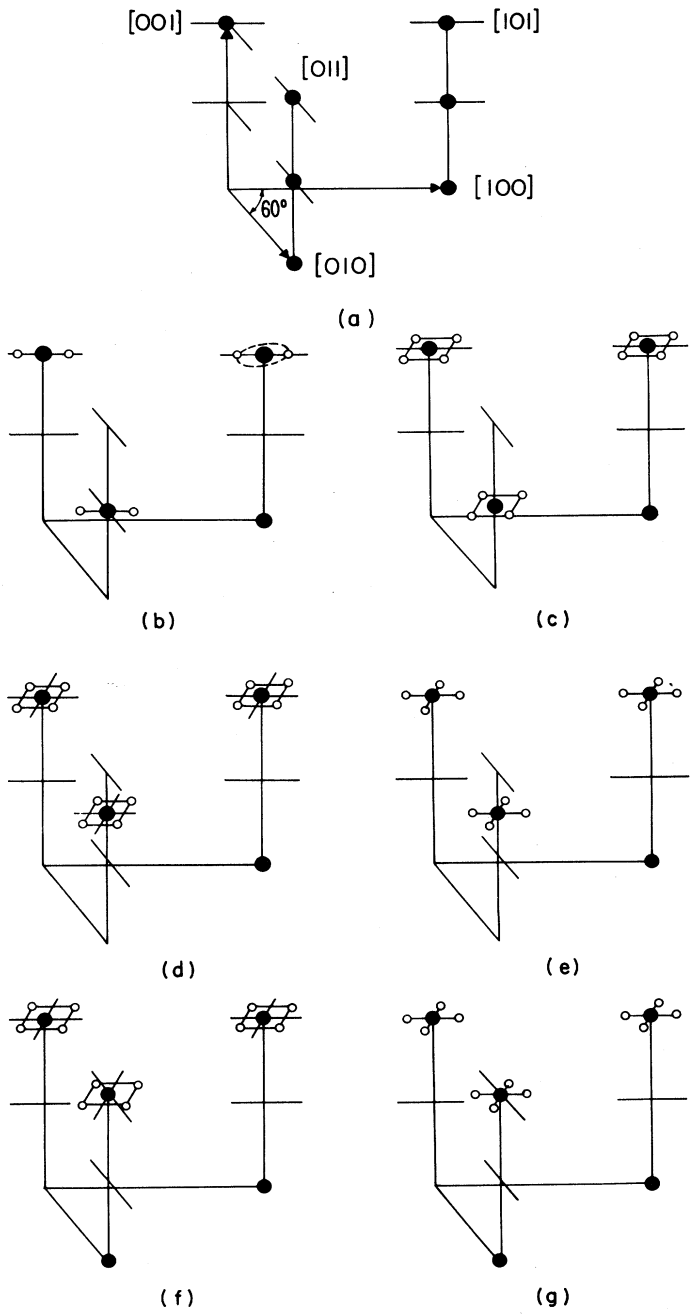

FIG. 2. Reciprocal-space structure of the observed crystalline-B phases. The solid dots represent the principal Bragg peaks related to the stacking structure. The open dots represent the satellite peaks caused by the modulation. Only two of the six hexagonal directions are shown here, and only for positive L. Only first-order modulation reflections are shown here. The lines are guides for the eye. (a) $ABAB$, 64→69 °C. No ordered modulations, therefore, no satellites. All six hexagonal directions are equivalent. (b) Ortho-$m1$, 62.5→64 °C. $\mathbf{q}$ is along the [100] direction. Note that there are no satellites on the $L=0$ peak. The [100] and $[\bar{1}00]$ directions are equivalent and the [010], $[0\bar{1}0]$, $[\bar{1}10]$, and $[1\bar{1}0]$ directions are equivalent. The dotted line is the path mapped out by a circle scan. (c) Ortho-$m2$, 61.5→62.5 °C. $\mathbf{q}$'s are at ±45° to the [100] direction. $|\mathbf{q}_1| = |\mathbf{q}_2|$. (d) Mono-$m2$, 61.0→61.5 °C (observed on cooling from ortho-$m2$ and heating from AAA-$m2$). There are peaks at $[01(1-s)]$ and not shown at $[01(-s)]$, $[0\bar{1}s]$, and $[0\bar{1}(-1+s)]$, where s decreases from $\frac{1}{2}$ to 0 as the temperature is lowered. The pairs of directions [100]-$[\bar{1}00]$, [010]-$[\bar{1}10]$, and $[0\bar{1}0]$-$[1\bar{1}0]$ are equivalent. (e) Mono-$m3$, 61.0→61.5 °C (observed only on heating from the AAA-$m3$ phase). (f) AAA-$m2$, 55→61 °C (observed on cooling from ortho-$m2$). All six hexagonal directions are equivalent. Peaks only at integral L values. (g) AAA-$m3$, 55→61 °C (observed only on quenching from ortho-$m1$). $\mathbf{q}$'s are at 0 and 90° to the [100] direction. $|\mathbf{q}_1| = |\mathbf{q}_2|$.

A triple-axis spectrometer with LiF[200] crystals as monochromator and analyzer was used. The spot size on the film was 2.5×2.0 mm^2 and the zero arm in a nondispersive geometry had a FWHM of 0.09°. This gave us a resolution in the plane of the layers (ΔH) of 0.002 H units (0.003 Å^{-1}) and a resolution normal to the plane of the layers (ΔL) of 0.004 L units (0.0008 Å^{-1}). The vertical resolution, determined primarily by slits, was 1° in χ at $2\theta=20°$ which corresponds to 0.017 H units (0.025 Å^{-1}). We made use of three different reciprocal-space scan types to characterize the stacking sequence of the sample. The χ scans rotated the film about the layer normal and corresponded to a circular path in reciprocal space about the [001] direction. This scan revealed the in-plane domain structure. The H scan traced a path normal to the [001] direction and was used to measure the in-plane lattice constants. The L scan traced a path parallel to the [001] direction and was used to determine the stacking structure. Special reciprocal-space scans which moved 2θ, θ, and χ were designed to study the satellite structures, by moving in circles of arbitrary radius in an ($00L$) plane about a ($10L$) Bragg peak (circle scans) and through arbitrary diameters of those circles (diameter scans).

A quantitative procedure was developed for determining the number of layers in films of intermediate thickness, (i.e., 30–200 layers) by observing the film color when white light is reflected. The thickness of the thicker films was measured using the scattered intensity of x rays in the sample's Sm A phase. The details of the procedure for thickness determination are contained in the companion paper.[1]

EXPERIMENTAL RESULTS

We will present data demonstrating that between approximately 60 and 65 °C there are four different stacking sequences in bulk 7O.7 with three different modulation structures, resulting in seven different phases. These are illustrated in Fig. 2. As mentioned above, the three independent sets of evidence to support these conclusions are the x-ray studies on bulk samples of the layer spacing and the modulation-induced satellites on the (001) peak, and the free film studies of the satellites on the ($10L$) peaks.

The reciprocal-space structures sketched in Fig. 2 are observed directly on monodomain thick films. To simplify the drawings, only the ($10L$), ($01L$), and (001) peaks and their satellites are shown. The stacking structures at the various temperatures were determined from the positions of the principal Bragg peaks in the L scans at ($10L$) and ($01L$). The satellite positions about the ($10L$) and ($01L$) peaks were measured directly using the special circle and diameter scans described above and shown in Fig. 3. The curve in reciprocal space mapped out by a typical circle scan is shown in Fig. 2(b). The circle scans show unambiguously the orientation of the satellites with respect to the lattice. The satellites shown at (001) are implied from the powder data taken at that peak. The powder data, which will be presented below for each phase along with the free-film data, are consistent with the (001) satellites having the same structure as the satellites about the other peaks. The detailed descriptions of the four stacking sequences along with typical L scans is contained in Collet *et al.*[9,10] and Sirota *et al.*[1]

Figure 2(a) displays the principal Bragg peaks for the $ABAB$ phase.[2–4] This phase has no long-range modulation, so there are no sharp satellites around these peaks. The existence of peaks at $L=\pm\frac{1}{2}$ corresponds to the two-layer repeat distance of the structure which has two molecules per unit cell. The ratio of the intensities of the half-integer L peaks to the integral L peaks is close to the ratio of 3 to 1 which is predicted from the structure factor when molecular form factor and Debye-Waller effects are neglected.

The ortho-$m1$ (Or-$m1$) phase [Fig. 2(b)] is the same phase as the modulated orthorhombic phase described by Collet *et al.*[9,10] This structure has one molecule per primitive unit cell. The circle scan presented in Fig. 3(a) shows the orientation of the satellites. Circle scans were also taken about the other Bragg peaks and the satellites were all oriented along the [100] direction. The measured ratio of the intensity of the satellites to that of its principle Bragg peak was such that the satellites about the $L=\frac{1}{2}$ peaks were weaker by a factor of ~4 and

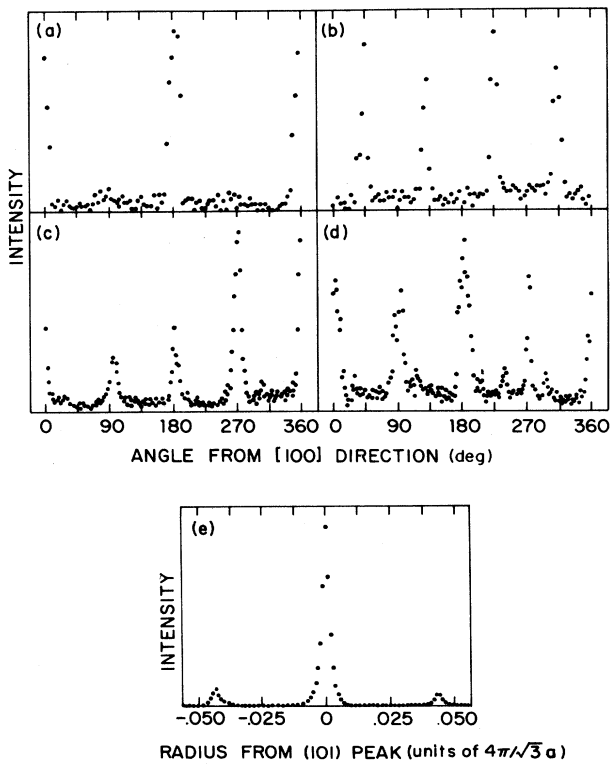

FIG. 3. (a)–(c) Circle scans in the (001) plane, about the (101) peak, with a radius of ~0.05 H units. They are in the ortho-$m1$, ortho-$m2$, and AAA-$m3$ phases, respectively. (d) Circle scan as above, with radius of ~0.07 H units in the ortho-$m2$ phase. This shows the second-order mixed peaks $|\mathbf{Q}\pm\mathbf{q}_1\pm\mathbf{q}_2|$. (e) Diameter scan through the (101) peak, along the [100] direction, in the AAA-$m3$ phase. This shows the Bragg peak and the modulations with $\mathbf{q}\simeq0.046$ H units.

there were no satellites observed at $L=0$. This is consistent with the satellite ratio scaling as L^2 [i.e., $(\mathbf{Q}\cdot\mathbf{u})^2$]. The observation that the satellites about all six of the principal hexagonal directions are aligned in the same direction, tells us that the modulation consists of a single wave vector ($\mathbf{q}$) and possible harmonics. The fact that these satellites do not appear on the (100) peak demonstrates that the modulation is polarized along the [001] direction.[4,9,11] Accompanying the lack of hexagonal symmetry in the stacking and modulation is a distortion of the average reciprocal lattice such that the in-plane reciprocal-space length of the (100) peak is greater than that of the $(01\frac{1}{2})$ and $(\bar{1}1\frac{1}{2})$ peaks by about 0.1%. While we continue to index the peaks as (100), (010), etc., the actual H and K values for the peaks vary slightly due to thermal expansion, as well as this distortion. Thus, at the high-temperature end of this phase the in-plane reciprocal length for the (100) peak was 0.9990 ± 0.0001 H units, while for the $(01\frac{1}{2})$ peak it was 0.9981 ± 0.0001 H units.

The satellite structure was independently confirmed by the presence of satellites on the (001) peak in unoriented samples. Let $\mathbf{q}=q\hat{\mathbf{x}}$ be the modulation wave vector and Q be the magnitude of the [001] wave vector. For an unoriented sample we would observe the satellite at scattering angle 2θ given by

$$2k_0 \sin\left[\frac{2\theta}{2}\right]=(Q^2+q^2)^{1/2}\approx Q+\frac{q^2}{2Q}\ .$$

Figure 4(a) shows the principal (001) Bragg peak at $2\theta=2.885°$ for $T=65.2$ °C in the $ABAB$ phase. In addition, there is a weak diffuse peak near the position at which the resolution-limited satellites are observed in the ortho-$m1$ phase. Figure 4(b) shows the principle Bragg peak at $2\theta=2.885°$ and the satellite, at a 2θ that is larger by 0.18°, for $T=63.5$ °C in the ortho-$m1$ phase. The modulation wave vector corresponds to $q/Q=0.35$. Since the units of H are seven times those of L, the wave vector of the modulation $q=0.050$ H units corresponds to a wavelength of about 20 molecules. The change from a broad diffuse peak to a resolution-limited line shape occurs abruptly at the transition from the $ABAB$ to the ortho-$m1$ phase.

On cooling from the ortho-$m1$ phase, we observe a first-order transition with hysteresis of ~0.5 °C at ~62.5 °C, to a new phase whose reciprocal-space structure is shown schematically in Fig. 2(c). From the nominally unchanged positions of the principal Bragg peaks, we see that the stacking structure of the molecules is unchanged and remains orthorhombic. The distortion of the reciprocal lattice, which had become larger as the temperature was decreased within the ortho-$m1$ phase, collapsed at this phase transition by about a factor of 4, causing the in-plane reciprocal-lattice values to be different by only ~0.0003 H units. The most dramatic change occurring at this transition is in the satellite structure. A circle scan about the (101) peak at a reciprocal-space radius of q shows the new structure in Fig. 3(b). One should compare this structure to that of the ortho-$m1$ phase shown in Fig. 3(a). We call this new

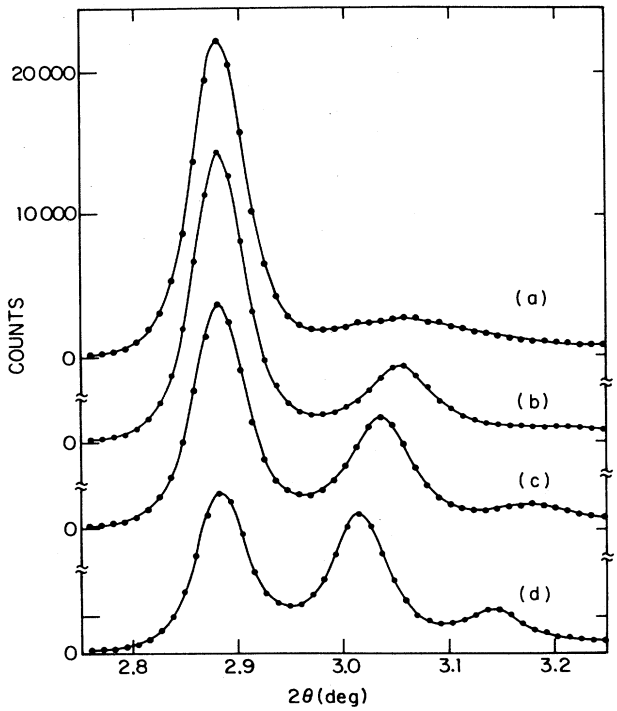

FIG. 4. 2θ scans of powder sample with position sensitive detector. The peak at $2\theta=2.88°$ is the resolution-limited (001) Bragg peak. (a) $ABAB$, $T=65.2$ °C. A weak diffuse peak is observed at the satellite position. (b) Ortho-$m1$, $T=63.5$ °C. The sharp satellite appears. (c) AAA-$m2$, $T=60.8$ °C. The satellite has grown stronger and the peak due to scattering at $|\mathbf{Q}\pm\mathbf{q}_1\pm\mathbf{q}_2|$ is clearly visible. The satellite is clearly resolution limited here. (d) AAA-$m2$, $T=56.7$ °C. The satellite is even stronger.

modulation structure $m2$. The structure goes from one with a single wave vector $\mathbf{q}$ along the [100] direction, to one with two wavevectors $\mathbf{q}_1$ and $\mathbf{q}_2$ with equal magnitudes, oriented at ±45° to the [100] direction;

$$\mathbf{q}_1=(1,+1,0)\frac{q}{\sqrt{2}},\quad \mathbf{q}_2=(1,-1,0)\frac{q}{\sqrt{2}}\ .$$

The fact that these are two spatially coincident modulations, and not single modulations coming from different domains, is demonstrated by the existence of weaker satellite peaks at $\mathbf{Q}\pm\mathbf{q}_1\pm\mathbf{q}_2$ which near the (101) peak occur at $(1\pm\sqrt{2}q,0,1)$ and $(1,\pm\sqrt{2}q,1)$. These peaks are not portrayed in Fig. 2; however, a circle scan at a reciprocal space radius of $\sqrt{2}q$ shows them in Fig. 3(d).

This structure is also confirmed by measurements of the unoriented powder sample, which, in addition to peaks at $2k_0\sin(2\theta/2)=Q$ and $Q+q^2/2Q$, has one at $Q+q^2/Q$ corresponding to the four peaks at $\mathbf{Q}\pm\mathbf{q}_1\pm\mathbf{q}_2$ [Figs. 4(c) and 4(d)]. A weak peak due to scattering from $\mathbf{Q}\pm2\mathbf{q}_1$ and $\mathbf{Q}\pm2\mathbf{q}_2$ was observed at lower temperatures. The intensities of these higher-order satellites cannot be used to determine the local waveform of the modulation because they are reduced by a Debye-Waller factor caused by the phase and amplitude variations of

the modulation.

When the sample was cooled from the ortho-$m2$ (Or-$m2$) phase, the $m2$ modulation structure was observed to persist through the mono [Fig. 2(d)] and AAA [Fig. 2(f)] phases. The (101) peak and its satellites were unchanged across these transitions. The L value of the $(01L)$ peak (which is 0.5 in the orthorhombic phase), increases through the monoclinic phase and becomes 1.0 in the AAA phase. The details of the stacking structure in the monoclinic phase are described in Collett *et al.*[10,9] the satellites about the $(01L)$ peak move along L with it, unchanged, except that the satellite-to-Bragg-peak intensity ratio increases consistently with the expected L^2 dependence. (The mirror image peak moves from $L=0.5$ to $L=0$.) Transitions between the ortho-$m2$, mono-$m2$, and AAA-$m2$ phases are all observed to be first order and reversible.

Rapid cooling (i.e., quenching) from the ortho-$m1$ phase to a temperature in which the stacking is AAA, results in a third ($m3$) satellite structure. The structure of the AAA-$m3$ phase is shown in Fig. 2(g) and circle and diameter scans are shown in Figs. 3(c) and 3(e). Like the $m2$ structure, the $m3$ structure contains two spatially coincident modulations with wave vectors of equal magnitude and at right angles to each other; however, their orientation is rotated 45°. One wave vector points along the [100] direction (as the $m1$ modulation does) and the other is oriented at 90° to it. This phase appears to be stable on the time scale of at least a few days. Heating from the AAA-$m3$ into the monoclinic phase resulted in the mono-$m3$ phase [Fig. 2(e)]. Heating this into the lower orthorhombic region yielded the ortho-$m2$ phase. When heating from the CrG phase to the CrB-AAA phase, the poor mosaic prevented us from taking high-quality data; however, the circle scans appeared to contain evidence of both $m2$ and $m3$ modulation structures.

Although there is no measurable temperature dependence to the magnitude of $q \approx 0.05H$ for the $m1$ modulation, with decreasing temperature through the other modulated phases the magnitude of the wave vectors does decrease to $\sim 0.04H$ in both the $m2$ and $m3$ phases. This is shown in Fig. 5(a). Due to the problem of correctly orienting the domain to be studied in the free-film measurements, the data for $|\mathbf{q}|$ in the powder-sample measurements are more precise. They do agree, however.

The ratio of the intensities of the satellite peaks to the Bragg peaks is determined by both the amplitude and the exact waveform of the modulation. Taking $\mathbf{Q}$ to represent the wave vector for the (001) Bragg peak, the ratio of the intensity of the satellites at $\mathbf{Q}\pm\mathbf{q}$ to that of the Bragg peak at $\mathbf{Q}$ is given by

$$\frac{\left|\sum_i \exp\{i[\pm\mathbf{q}\cdot\mathbf{R}_i+\mathbf{Q}\cdot\mathbf{u}(\mathbf{R}_i)]\}\right|^2}{\left|\sum_i \exp[i\mathbf{Q}\cdot\mathbf{u}(\mathbf{R}_i)]\right|^2},$$

where we have made use of the fact that $\sum_i \exp[i(\pm\mathbf{q}\cdot\mathbf{R}_i)]=0$. To lowest order in $\mathbf{u}$ this can be written as

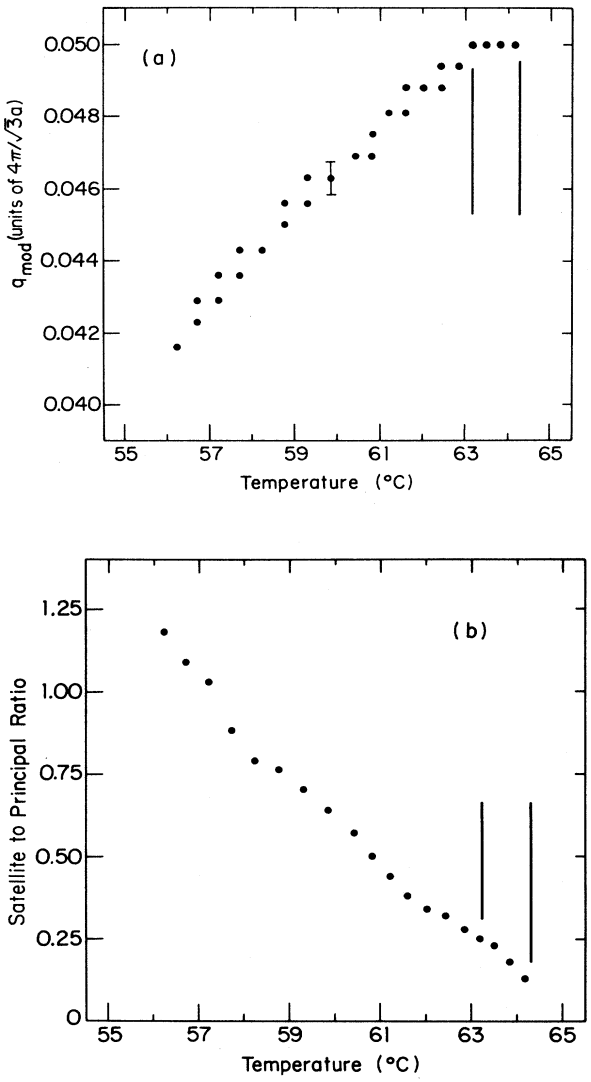

FIG. 5. (a) Temperature dependence of the magnitude of the modulation wave vector. The data plotted are taken from the unaligned sample measurement. A typical error bar is shown. The film data are consistent with this and no difference between the values in the $m2$ and $m3$ phases could be shown. (b) The temperature dependence of the intensity of the satellites relative to the peak. These are data from powder sample (see text for film data and uncertainties). Remember that the $m2/m3$ phases have four satellite peaks while the $m1$ only has two. The vertical lines denote the transitions between ortho-$m2$, ortho-$m1$, and $ABAB$.

$$\frac{\left|\sum_i [i\mathbf{Q}\cdot\mathbf{u}(\mathbf{R}_i)]\exp[i(\pm\mathbf{q}\cdot\mathbf{R}_i)]\right|^2}{\left|\sum_i 1\right|^2}.$$

The measured ratio of the intensity of the satellite to that of the Bragg peak is shown in Fig. 5(b) for the powder data. Since there are four satellites per Bragg

peak for the $m2$ and $m3$ modulated phases, the measured ratio is four times that of the ratio for a single peak. For the ortho-$m1$ phase the multiplicity is only 2. Looking at Figs. 4(a) and 4(b), one can see that there is some ambiguity in the choice of the background because of diffuse scattering and, therefore, the values plotted in Fig. 5(b) may not be exact. What is important in these data is the fact that the ratio is a monotonically increasing function of temperature and that there is no noticeable jump at the ortho-$m1$–to–ortho-$m2$ transition. Since the multiplicity increases from 2 to 4, this implies that the intensity of an individual satellite in the ortho-$m2$ phase is $\frac{1}{2}$ of the intensity of a satellite in the ortho-$m1$ phase at the transition.

The intensity ratios measured with the free-film sample were much more uncertain because of the difficulty in locating the positions of both the Bragg and satellite peaks and then confirming that there were not other satellites at multiples of $\pm 60°$ in χ orientation, arising from a single-crystal domain with its modulation structure broken into multiple domains. In addition, since χ rotation invariably changed the part of the sample that was illuminated with x rays, there were further uncertainties.

As temperature is lowered through the ortho-$m1$ phase the intensity ratio (per satellite peak) measured on free films increases from 0.03 ± 0.01 to 0.06 ± 0.01. When cooling into the ortho-$m2$ phase from the ortho-$m1$ phase, the ratio drops precipitously to 0.035 ± 0.01 and then increases continuously to 0.05 ± 0.01 as the temperature is lowered to the bottom of the ortho-$m2$ phase. Cooling through the AAA phase, the ratio increases from 0.06 ± 0.01 at its highest temperature to 0.16 ± 0.05 before becoming CrG. We have consistently observed that the relative intensities of satellite to (001) Bragg peak as observed in the powders is higher than that observed for the (10L) peaks by nearly a factor of 2. Although this could be due to the domain structure, we suspect it may be a real effect due to different Debye-Waller factors for the satellites at the (q01) and the ($1\pm q,0,L$) reciprocal-space positions. In any event, the increasing ratio with decreasing temperature is quite clear in both sets of data. Furthermore, both sets of data are also consistent with the continuity of the ratio across the ortho-$m1$–to–ortho-$m2$ transition. We will refer to this last point below. Although there were variations in the film data for the relative intensities of the two or four satellites around a Bragg peak, we believe that they can all be explained by multiple χ domains within the illuminated volume.

The difference in the in-plane reciprocal-lattice vectors (in H units) for the (101) and (01$\frac{1}{2}$) peaks is plotted in Fig. 6 for both the thick and thinner films. On cooling a thick film, the distortion in the ortho-$m1$ phase is $\sim 0.09\%$ at the transition and increases to $\sim 0.15\%$ as the temperature is lowered. At the transition to ortho-$m2$ it drops to $\sim 0.03\%$. Previously, the drop in distortion was mistakenly identified with the orthorhombic-to-monoclinic transition.[9,10] The distortion in the mono-$m2$ phase is approximately the same as that in the ortho-$m2$ phase; however, it has not been studied carefully throughout the mono phase. As film thickness is

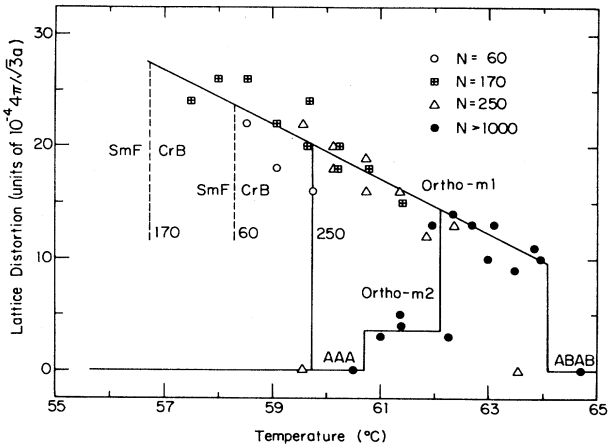

FIG. 6. The distortion of the reciprocal lattice as a function of temperature for different-thickness films. The lines are guides for the eye. On cooling, the 60- and 170-layer films become smectic-F (at temperatures denoted by the dashed vertical lines) before the distortion disappears. The AAA and $ABAB$ phases have no distortion. The ortho-$m1$ has a distortion which increases with decreasing temperature as long as the phase persists. The ortho-$m2$ has a small finite distortion. The nature of the distortion in the mono phase has not been determined.

decreased, the ortho-$m1$ phase persists to lower temperatures and the lattice distortion continues to increase with decreasing temperature until the lattice becomes either AAA with no peak at $L=\frac{1}{2}$, for thick films, or the sample becomes SmF for thinner films.[1] This is consistent with the low-resolution result[16] that the orthorhombic phase persists to lower temperatures; however, we now have evidence that it is specifically the ortho-$m1$ that is persisting.

In films thinner than ~ 200 layers, the low-resolution data showed evidence of a phase with ABC stacking between the $ABAB$ and the orthorhombic phase.[1] The films were mechanically unstable in this phase and tended to rupture, while films of the same thickness in the $ABAB$ or ortho phases were extremely stable. We note here that in bulk samples, the homologous compound 5O.6 has an ABC phase between the $ABAB$ and ortho.[12] In spite of the fact that certain aspects of the data presented here do not agree with the details of the theory presented by Hirth *et al.*,[14] the appearance of ABC stacking in thinner films of 7O.7 gives support to the basic idea of that theory. The powder data show evidence of a diffuse modulation at temperatures above the ortho-$m1$ phase. This is similar to analogous data for the 5O.6 ABC phase which is known[13] to exhibit an unoriented diffuse modulation in the plane of the layers. The weak diffuse peak that can be seen in the powder data of Fig. 4(a) suggests that the $ABAB$ phase of 7O.7 also exhibits a similar diffuse modulation structure. On further decrease in thickness the tilted hexatic SmI and SmF phases replace the crystalline ABC phase.

The results of the high-resolution measurement of the interlayer spacing of a magnetically aligned bulk sample

shown in Fig. 7 indicate that the layer spacing decreases by only 0.07% across the entire Cr*B* range. The largest temperature-dependent tilt that would be consistent with this is less than 1°. The error bars in Fig. 7 correspond to a maximum tilt of 0.8°. Since there is also no observable discontinuity near the *ABAB*-to-ortho-*m*1 transition, the molecular tilt changes by less than 1° across this transition. This result is inconsistent with the explanation in Hirth *et al.*[14] for the measured distortion of the lattice constants in the orthorhombic phase. In the following section we describe a model for the modulation structures that is consistent with the above result, explains both the period of the modulation and the lattice distortion, and also incorporates the dislocation argument in a slightly different form.

At this point we need to describe the detailed structure of the Cr*G* phase.[7,5,20,1] Each layer consists of molecules packed in a distorted hexagonal arrangement. The molecules are tilted with respect to the layer normal by 22°→25° (temperature dependent).[7] The tilt in the smectic-*F* (Sm*F*) phase ranges from ~19.5° to 22°, being continuous across the Sm*F*-to-Cr*G* transition.[21] In the present *HKL* units peaks are observed at (0.925,0,2.6) and (0,0.98,1.3). Using the common crystallographic notation the lattice parameters relevant to these units are $a=9.45$ Å, $b=5.15$ Å, $c=30.6$ Å, and $\beta=111.9$ Å. The distortion of the in-plane lattice is almost what would be computed from the tilting of rigid cylinders. If it were exactly so, the scattering vectors of both peaks would have equal magnitudes. This has been measured and they are not equal. In terms of the scattering angle, the splitting is $\Delta(2\theta)/2\theta=0.0075\pm0.0005$ where the 2θ is larger for the peak in the reciprocal-space direction that is in the plane containing the layer normal and the tilt direction. This tells us that if the molecules are packed end to end (see companion paper[1]) the long axes of the pairs of molecules which are displaced from each other along those axes, lie closer to each other by 0.75% compared to pairs of molecules which are not so displaced. A similar distortion was observed for the Cr*G* phase of the homologous compound [4-(*n*-pentyl)oxybenzylidene]-4-(*h*-hexyl)aniline (9O.4). Such distortions were suggested by Leadbetter *et al.*[5]

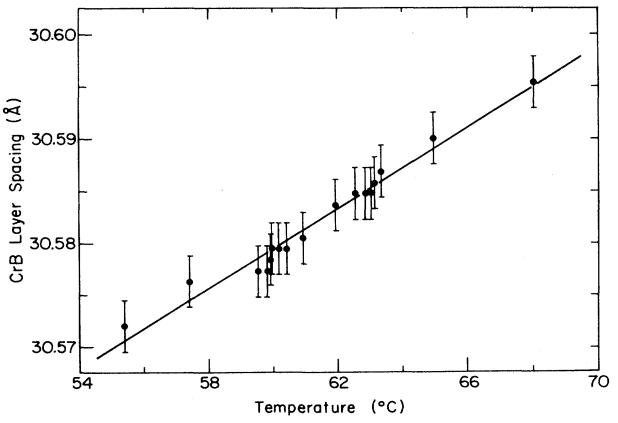

FIG. 7. Temperature dependence of the layer spacing. The straight line is a fit.

Our powder data showed evidence of a weak satellite about the (001) peak in the Cr*G* phase as well. At $T=53$ °C the main peak was at $2\theta=3.09°\pm0.03°$ and the satellite was at $2\theta=3.24°$ with an intensity of ~10% that of the main peak. As the temperature was lowered the satellite grew weaker and moved closer to the main peak until it was not observable. Since this satellite was weak and since it was not possible to obtain a good mosaic in the Cr*G* phase, we were unable to characterize this satellite in more detail or to determine the orientation of its wave vector.

MODEL

In all cases that we are familiar with, the appearance of long-wavelength modulations in thermal equilibrium is due to some sort of local frustration that is partially relieved by a more macroscopic inhomogeneity, or modulations.[22–24] It is likely that the modulated phases described here have a similar origin. Although the model proposed by Hirth *et al.*[14] explained the appearance of a modulation at the transition from the *ABAB* to the ortho-*m*1 phases in terms of a martensitic mechanism, it did not explain the period of the modulation. According to this model a long-wavelength metastable configuration was required in order to relieve the macroscopic shear accompanying a local structural transformation. The difficulty with this model is that since the same modulated phase (the ortho-*m*1) is observed to appear reversibly on both heating and cooling and since in this, and the other, modulated phases, the modulation wave vector appears to be a function of only temperature and not sample history, the modulated structures must be in thermal equilibrium rather than being metastable. However, we do believe that the Hirth model was correct in attributing the transformation to a set of partial dislocations that transform the *ABAB* phase into one that is nearly *ABC*. We say nearly *ABC* since the data described above for the (001) layer spacing clearly demonstrates that the molecules do not tilt by the ~2.75° by which the layers tilt. On the other hand, the appearance of the *ABC* phase in films below ~250 layers, at temperatures between the *ABAB* and the ortho-*m*1, supports the essence of the Hirth model. Figure 8 describes a variation on the Hirth model that has further experimental support.

In place of alternate regions of local *ABC* and *ACB* stacking, with layers tilted in opposite directions by ~2.75 °C (at the *ABAB*-to-ortho-*m*1 transition) we propose regions of either *ABC* (or *ACB*), tilted by the same angle, but separated by walls in which the local intralayer packing is the same as that in the Cr*G* phase and where the local layer normal is tilted by ~23° to the long molecular axis. (Note that in the Cr*G* phase, the angle between the molecular axis and the layer normal is ~23°.) Also note that in contrast to the Hirth model, and in agreement with the new experimental facts, in this model the molecules are *not tilted* with respect to the *average* layer normal.

There are two separate experimental facts supporting this model. Firstly, if one assumes that the average layer tilt is constant across the *ABAB*-to-ortho-$m1$ transition (see Fig. 9), then the ratio of the lengths $(\lambda-\delta\lambda)/\delta\lambda$ must be equal to the ratio $\tan(23°)/\tan(2.75°)$. Taking $\delta\lambda=2$ molecular spacings yields $\lambda=19.7$ molecular spacings where the measured value is 20.0 ± 0.4. Assuming that the CrG-like packing arises as a relatively low-energy "defect structure," then $\delta\lambda=2$ is the smallest wall for which that packing is realized for one molecule. Secondly, we know that the experimentally measured anisotropy of the lattice spacing in the CrG phase is such that in the plane normal to the molecular axis, the nearest-neighbor distance along the direction of the molecular tilt is 0.75% smaller than in the other directions. If the same packing holds true for the wall of CrG-like packing in the modulated structures, then in the ortho-$m1$ phase, the in-plane component of the average reciprocal-lattice vector for the (101) peak should be greater than that of the $(01\frac{1}{2})$ peak by $0.0075\times\delta\lambda/\lambda=0.000\,83$ H units. The experimentally observed value is 0.0009 ± 0.0001 H units. Although these two facts are not sufficient to rule out other possible models they do justify further speculation as to the molecular mechanisms that could give rise to the model illustrated in Fig. 8.

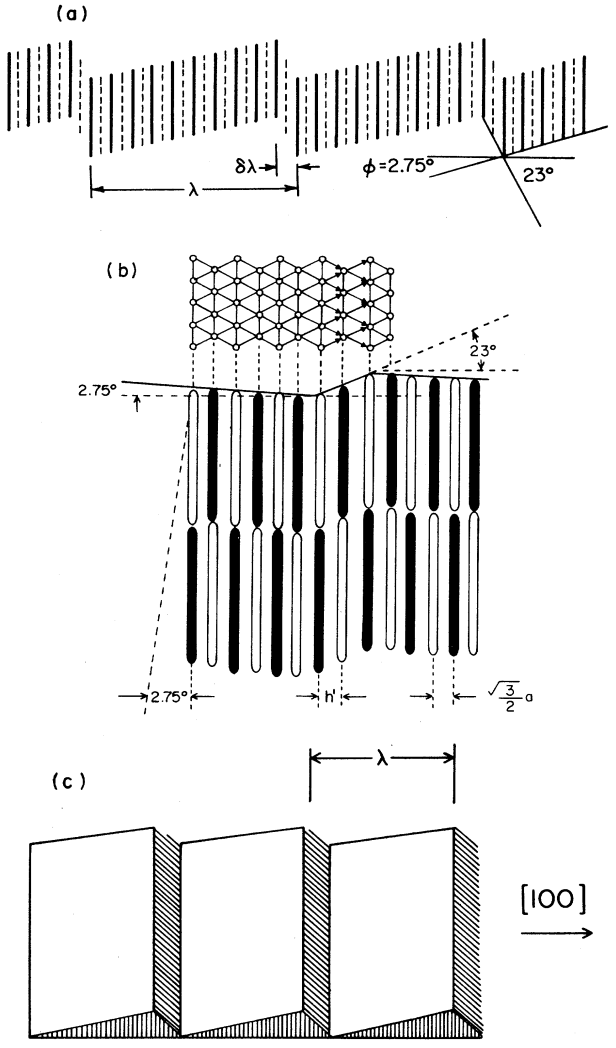

FIG. 8. (a) Schematic (not to scale) representation of the relation between the local layer tilt and the wave length of the modulation in the ortho-$m1$ phase. Solid lines represent molecules that are in the plane of the page and the dotted lines are for molecules out of the plane. (b) A magnified view of the section of (a) in the vicinity of the wall, together with a top projection $[h'=0.9925(\sqrt{3}/2)a]$. The molecules represented by solid bars are in the plane of the page. This should be compared with Fig. 9 for the CrG phase. (c) A schematic illustration of the layer topology for the modulations of the ortho-$m1$ phase. Compare this to the $m2$ structure illustrated in Fig. 10.

If the molecules are imagined to be rigid cylindrical rods, then in the *ABAB* phase the rods are side by side in such a manner that they form layers whose normals are parallel to the axis of the rods. The interlayer spacing is such that the molecules in any one layer "sit" at sites that are interstitial to the ends of the rods in the adjacent layers. This packing results in two molecules per unit cell. In contrast, in the CrG phase the near-neighboring molecules are displaced along the rod axis in such a way that the normal to the layers makes an angle of $\sim23°$ to the rod axis. The CrG layers are then stacked in such a way that the ends of the molecules in one layer point directly toward the ends of the molecules in the adjacent layers. There is only one molecule per unit cell for this stacking. Figure 9 is a schematic representation of the CrG phase, showing projections normal to the rod axis (i.e., normal to the nematic director) and from the side. The arrows between molecules in the pro-

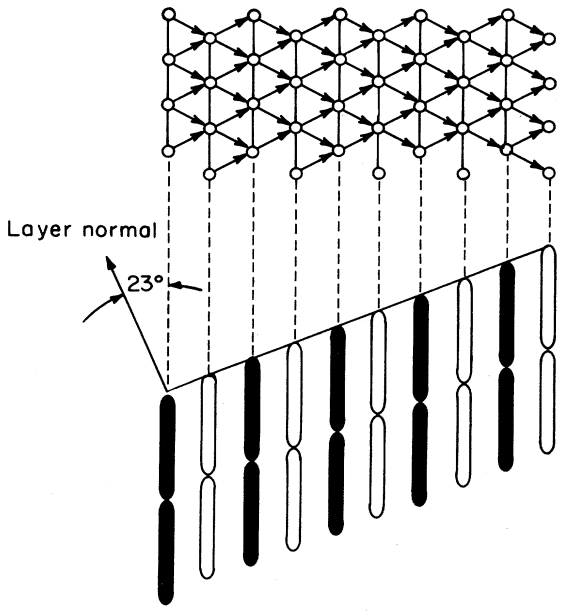

FIG. 9. CrG phase structure. Top and side view. In the top view the arrows on the lines refer to the fact that the molecules they join are displaced with respect to each other in the direction normal to the paper.

jection normal to the director denote the fact that for these molecules the relative displacements along their long axis is approximately 6% of their length. Measurements in the Cr*G* phase tell us that the nearest-neighbor distance in this projection for molecules connected by arrows is shorter than for other neighbors by 0.75%.

According to both the original Hirth model, and the present model as well, the *ABAB*–to–ortho-*m*1 transition is accompanied by a change in local packing from *ABAB*, with two molecules per unit cell, to *ABC* (or *ACB*) with only one molecule per unit cell. In the original Hirth model the molecules tilted along with the layers such that the ends of the molecules in one layer remained at the geometric center of the interstices formed by the ends of molecules in the adjacent layer. We have seen above that the data rule out this possibility. In the present model the molecules maintain their original orientation and only the layers tilt. The local *ABC* stacking has the result of bringing the ends of the molecules in one layer nearer to the ends of some of the molecules in the adjacent layer. Thus one possible microscopic mechanism for driving the *ABAB*–to–ortho-*m*1 transition might be an attractive interaction between the ends of molecules in adjacent layers. In fact, the restacking sequence from the *ABAB*, through the orthorhombic, monoclinic, and *AAA* phase is a continuous progression in which end-to-end distances become smaller. The simplest model of the Cr*G* and Cr*B*-*AAA* phases would have the ends of the molecules in adjacent layers touching each other. According to this picture the principal difference between Cr*G* and the *AAA* phases would be in the nearest-neighbor displacements depicted in Fig. 9 for the Cr*G* phase. On the other hand, the present model for the ortho-*m*1 phase attributes a local layer tilt of 2.75°. This implies that the neighboring molecules in the ortho-*m*1 phase have similar, although smaller, displacements than the molecules in the Cr*G* phase. Since the present model, and the one proposed by Hirth, both propose similar layer tilts in both the ortho-*m*1 and the *AAA* phase, the difference in the displacements of neighboring molecules in the modulated Cr*B* phases and the Cr*G* is more of a quantitative one concerning the magnitude of the relative displacements, rather than the qualitative symmetry distinction that characterizes the simple model. Although we do not have an argument that can differentiate the relative importance of the molecular displacements of neighboring molecules within a layer, in comparison with the end-to-end distances for molecules in adjacent layers, it is reasonable to suggest that, in some combination, these two effects reflect the microscopic interactions that drive the restacking transitions. Since the modulation is a longer-range effect, we suspect that is must be explained separately.

One likely origin for the modulation might be an incommensurability between the cross-sectional areas of the aliphatic chains and the aromatic cores. For example, although the cross-sectional area of the one-molecule unit cell in the hexagonal phases of 7O.7 and the cross-sectional area for the aromatic core ($\sim 3.5 \times 7.0$ Å^2) are both ~ 25 Å^2, the cross-sectional area for a straight aliphatic chain in the all transconfiguration is less than 10 Å^2.[25] The problem suggested by these numbers is not as serious as it appears since the long axis of the chains makes an angle of the order of 35° with the long axis of the aromatic cores. Thus the relevant chain cross-sectional area is ~ 19 Å^2/cos(35°)~ 23 Å^2. More serious, however, is the fact that there has to be a considerable amount of thermally induced rotational motion in order to obtain the observed nearly hexagonal macroscopic symmetry from molecules that are very asymmetric. Thus there must be a fairly delicate balance between the intramolecular energetics that determine the molecular conformation and the intermolecular interactions that determine the positions of neighboring molecules. Since aliphatic chains undergo "chain melting" transitions, which for appropriate chain densities occur in the same temperature range as the present restacking transitions,[26] it is reasonable to suggest that a third microscopic effect, in addition to the change in the end-to-end distances and the neighboring displacements, is a temperature-induced change in the ratio of the rotationally averaged cross-sectional areas of the chains and the cores. We suggest that when these areas are not equal there is a buildup of microscopic strains that require periodic walls in which the resultant macroscopic strain can be relieved. Without a more specific microscopic model we cannot explain why it is that the Cr*G* intralayer packing relieves that macroscopic strain. However, it is apparent that since the stable temperature range for the Cr*G* phase is only a few degrees away from the temperature of the restacking transitions, and since the enthalpy of the *AAA*-to-Cr*G* phase is not very large,[15] the microscopic energy cost for the Cr*G*-like wall is not large.

The observed sequence of restacking transitions and the accompanying modulations can be understood in terms of the previous ideas. The diffuse satellite peak that is seen in the powder data in Fig. 4(a) demonstrates the existence of uncorrelated modulations in the *ABAB* phase. As the temperature is lowered through the transition to the ortho-*m*1 phase the microscopic effects suggested above combine to produce the sawtoothlike modulation sketched in Fig. 8. We have argued above that this corresponds to walls with Cr*G*-like intralayer packing, two molecular spacings thick, and spaced approximately 20 molecular spacings apart. The fact that this modulation gives rise to resolution-limited satellites implies that the walls are well correlated over large distances. On further cooling within the ortho-*m*1 phase, the satellite intensity grows by nearly a factor of 2 without any observable change in the period of the modulation. For the present model this means that the layer tilt angle must increase by approximately $\sqrt{2}$. Since the only observable change in the (10*L*) Bragg peaks is an $\sim 50\% \pm 10\%$ increase in the splitting that is illustrated in Fig. 6, the macroscopically observed orthorhombic symmetry does not change. The primary microscopic change in this temperature range is thus an increase by approximately a factor of $\sqrt{2}$ in the relative intralayer displacement of neighboring molecules. If we invoke the argument that explained the splitting in terms

of the lattice spacings averaged over the modulation period, then the fact that the splitting increases by approximately 50% would be consistent with the average thickness of the CrG-like wall increasing to accommodate the $\sqrt{2}$ increase in the local layer tilt.

The main feature of the ortho-$m1$–to–ortho-$m2$ transition is the change in the modulation structure. It is straightforward to demonstrate that if the angle α of the local layer tilt is small, the two-dimensional modulation illustrated in Fig. 10 can be decomposed into two one-dimensional modulations, like that in Fig. 8(c) at $\pm 45°$ to the [100] direction and with tilt angles $\alpha/\sqrt{2}$. It follows that if the intensity of each of the two satellite peaks predicted from the one-dimensional modulation illustrated in Fig. 8(c) is proportional to $(\alpha\lambda)^2$, where α is the tilt angle, then the intensity of each of the four lowest-order satellite peaks predicted from the model for the two-dimensional modulation illustrated in Fig. 10 is proportional to $(\alpha\lambda)^2/2$. The fact that the sum of the intensities of the satellite peaks does not change at this transition demonstrates that the local tilt angle α also does not change. In the context of the present model the decomposition of the two-dimensional modulation into two one-dimensional modulations implies that the width of the CrG-like walls for the two-dimensional modulations are smaller by a factor of $1/\sqrt{2}$ than the width of the wall for one-dimensional modulation at this transition temperature. Note that the fact that the intensity of the satellites increases with decreasing temperature implies that according to the model the wall thickness also increases with decreasing temperature. At the onset of the ortho-$m2$ phase the walls for the two-dimensional modulation would therefore be two molecular spacings thick.

On further cooling to the onset of the AAA phase, the observed intensity of the satellites approximately doubles again. This implies that the local tilt of the layers at the onset of the AAA phase is twice (i.e., $\sqrt{2}\times\sqrt{2}$) that of the initial tilt in ortho-$m1$ (i.e., 5.5°). This is exactly the tilt increase which would result from the dislocations that Hirth *et al.* proposed for the orthorhombic to the AAA structure.[14] Since the CrG walls are perpendicular to each other in the ortho-$m2$ phase, we expect and measure a substantial decrease in the distortion of the lattice at the ortho-$m1$–to–ortho-$m2$ transition (Fig. 6). Continued cooling through the AAA phase results in a steady increase in both the period of the modulation and the intensity of the satellites until the first-order transition to the CrG phase.

We suspect that the $m3$ modulation has the same topology as the $m2$ modulation except that it is rotated by 45° so that the local tilt of the layers is at 45° to the [100] direction. On drop cooling from ortho-$m1$ to AAA, the local layer tilt need not be preserved since, unlike the orthorhombic structure, the local packing in the AAA structure does not distinguish between the [100] direction and the [010] or the [110] directions.

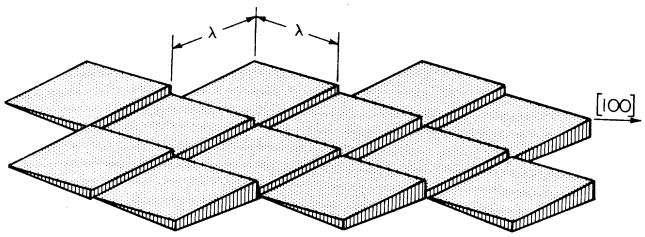

FIG. 10. Proposed structure for the $m2$ modulation. The $m3$ modulation has the same topology except that the [100] direction is shifted by 45°.

What we suspect is preserved on drop cooling are the walls of the $m1$ modulation, which are supplemented by the additional walls at 90°. On heating from the $m3$ into the orthorhombic region, the relation between the local layer tilt and the stacking structure requires that the tilt be along the [100] direction to yield an ABC packing of the centers of mass and presumably this causes the $m2$ modulation structure to return.

CONCLUSION

In summary, we have characterized the modulated phases in detail and presented a phenomenological model which can explain the observed results. In other homologous compounds it had been noted that the modulated phases appeared in the CrB phases of materials which had a lower-temperature CrG phase.[6,27] We have discussed possible mechanisms for that connection.

We have modified some details of the arguments made in Hirth *et al.*,[14] but have shown that the basic idea of ordered dislocation arrays remains applicable. Our data and model are also consistent with the shears and resultant layer tilts proposed by Hirth *et al.* to produce the orthorhombic and AAA structures from the $ABAB$. The occurrence of the ABC structure in thinner films is also a confirmation of that dislocation model.

This model may be of some relevance to other systems which show similar modulated structures, such as the modulated lyotropic lamellar phases[28] and the smectic-$\tilde{A}$ antiphase.[29]

ACKNOWLEDGMENTS

This work was supported by the National Science Foundation under NSF Grants Nos. DMR-85-13523 and DMR-83-16979. We would like to acknowledge J. Collett, L. B. Sorensen, and Kelby Chan for their assistance in the preparation of this experiment. We also gratefully acknowledge conversations with J. P. Hirth, J. Thoen, B. I. Halperin, and D. R. Nelson. One of us (M.D.) would like to acknowledge partial support from the United States–Israel Binational Foundation.

*Present address: Corporate Research Science Laboratories, Exxon Research and Engineering Company, Route 22 East, Annandale, NJ 08801.

†Permanent address: Physics Department, Bar-Ilan University, Ramat-Gan, Israel.

[1]E. B. Sirota, P. S. Pershan, L. B. Sorensen, and J. Collett, preceding paper, Phys. Rev. A **36**, 2902 (1987).

[2]D. E. Moncton and R. Pindak, Phys. Rev. Lett. **43**, 701 (1979).

[3]A. J. Leadbetter, J. C. Frost, and M. A. Mazid, J. Phys. (Paris) Lett. **40**, 325 (1979).

[4]A. J. Leadbetter, M. A. Mazid, B. A. Kelly, J. W. Goodby, and G. W. Gray, Phys. Rev. Lett. **43**, 630 (1979).

[5]A. J. Leadbetter, M. A. Mazid, and R. M. Richardson, in *Proceedings of the Bangalore Conference on Liquid Crystals, 1979* (Hayden, London, 1980).

[6]P. A. C. Gane, A. J. Leadbetter, and P. G. Wrighton, Mol. Cryst. Liq. Cryst. **66**, 245 (1981).

[7]J. Doucet and A. M. Levelut, J. Phys. (Paris) **38**, 1163 (1977).

[8]J. Doucet, A. M. Levelut, and M. Lambert, Phys. Rev. Lett. **32**, 301 (1974).

[9]J. Collett, L. B. Sorensen, P. S. Pershan, R. J. Birgeneau, J. D. Litster, and J. Als-Nielsen, Phys. Rev. Lett. **49**, 553 (1982).

[10]J. Collett, L. B. Sorensen, P. S. Pershan, and J. Als-Nielsen, Phys. Rev. A **32**, 1036 (1985).

[11]P. A. C. Gane and A. J. Leadbetter, J. Phys. C **16**, 2059 (1983).

[12]J. A. Collett, Ph.D. thesis, Harvard University, 1983.

[13]E. B. Sirota, J. Collett, P. S. Pershan, and L. B. Sorensen (unpublished).

[14]J. P. Hirth, P. S. Pershan, J. Collett, E. B. Sirota, and L. B. Sorensen, Phys. Rev. Lett. **53**, 473 (1984).

[15]J. Thoen and G. Seynhaeve, Mol. Cryst. Liq. Cryst. **127**, 229 (1985).

[16]E. B. Sirota, P. S. Pershan, L. B. Sorensen, and J. Collett, Phys. Rev. Lett. **55**, 2039 (1985).

[17]K. Chan, Ph.D. thesis, Harvard University, 1984.

[18]K. K. Chan, P. S. Pershan, L. B. Sorensen, and F. Hardouin, Phys. Rev. A **34**, 1420 (1986).

[19]C. Y. Young, R. Pindak, N. A. Clark, and R. B. Meyer, Phys. Rev. Lett. **40**, 773 (1978).

[20]A. J. Leadbetter, J. P. Gaughan, B. Kelly, G. W. Gray, and J. Goodby, J. Phys. (Paris) Colloq. **40**, C3-178 (1979).

[21]D. Guillon, A. Skoulios, and J. J. Bennatar, J. Phys. (Paris) **47**, 133 (1986).

[22]T. F. Rosenbaum, S. E. Nagler, and P. M. Horn, Phys. Rev. Lett. **50**, 1791 (1983).

[23]D. E. Moncton, J. D. Axe, and F. J. DiSalvo, Phys. Rev. B **16**, 801 (1977).

[24]P. Barois, C. Coulon, and J. Prost, J. Phys. (Paris) Lett. **42**, 107 (1981).

[25]S. A. Asher, R. Stearns, T. Urabe, and P. S. Pershan, Mol. Cryst. Liq. Cryst. **63**, 193 (1981).

[26]J. F. Nagle, Ann. Rev. Phys. Chem. **31**, 157 (1980).

[27]A. J. Leadbetter, M. A. Mazid, and R. M. Richardson, in *Liquid Crystals,* edited by S. Chandrasekhar (Cambridge University Press, London, 1980), pp. 5–79.

[28]W. K. Chan and W. W. Webb, Phys. Rev. Lett. **46**, 39 (1981).

[29]F. Hardouin, G. Sigaud, Nguyen Huu Tinh, and M. F. Achard, J. Phys. (Paris) Lett. **42**, L-63 (1981).

[30]E. B. Sirota, P. S. Pershan, S. Amador, and L. B. Sorensen, Phys. Rev. A **35**, 2283 (1987).